

# Analytical Expression for Continuum-continuum Transition Amplitude of Hydrogen-like Atoms with Angular-momentum Dependence

J B Ji<sup>1,\*</sup>, K Ueda<sup>1,2,†</sup>, M Han<sup>1,3</sup> and H J Wörner<sup>1,§</sup>

<sup>1</sup> Laboratorium für Physikalische Chemie, ETH Zürich, 8093 Zürich, Switzerland

<sup>2</sup> Department of Chemistry, Tohoku University, Sendai, 980-8578, Japan

<sup>3</sup> J. R. Macdonald Laboratory, Department of Physics, Kansas State University, Manhattan, KS 66506, USA

E-mail: \* [jiabao.ji@phys.chem.ethz.ch](mailto:jiabao.ji@phys.chem.ethz.ch), † [kiyoshi.ueda@tohoku.ac.jp](mailto:kiyoshi.ueda@tohoku.ac.jp), § [hwoerner@ethz.ch](mailto:hwoerner@ethz.ch)

**Abstract.** Attosecond chronoscopy typically utilises interfering two-photon transitions to access the phase information. Simulating these two-photon transitions is challenging due to the continuum-continuum transition term. The hydrogenic approximation within second-order perturbation theory has been widely used due to the existence of analytical expressions of the wave functions. So far, only (partially) asymptotic results have been derived, which fail to correctly describe the low-kinetic-energy behaviour, especially for high angular-momentum states. Here, we report an analytical expression that overcome these limitations. They are based on the Appell's  $F_1$  function and use the confluent hypergeometric function of the second kind as the intermediate states. We show that the derived formula can be applied to arbitrarily high angular momenta and quantitatively agrees with the numerical simulations using the time-dependent Schrödinger equation. Furthermore, we give an angular-momentum-dependent asymptotic form of the outgoing wavefunction and their continuum-continuum dipole transition amplitudes.

## 1. Introduction

The question ‘‘How long does the photoionisation take?’’ has intrigued researchers for decades ever since the early years of quantum theories. Its natural timescale of attosecond (as,  $10^{-18}$  s) has introduced a new field of science, known as the attosecond science, which is highlighted by the 2023 Nobel Prize in Physics [1]. The last 30 years have witnessed the rapid development of the toolbox for investigating the photoionisation processes with phase information embedded. This includes, but is not limited to, high-harmonic generation (HHG) [2, 3] as a table-top XUV source thanks to the availability of the high-power lasers, the schemes of performing the phase measurement such as attosecond streaking [4, 5, 6] and the reconstruction of attosecond beating by interference of two-photon transitions (RABBIT) [7, 8], and three-dimensional momentum-resolved particle detectors such as the cold target recoil ion momentum spectrometer (COLTRIMS) [9, 10, 11], and so on. As a result, it has become possible to measure the Wigner time delay defined as [12, 13, 14]:

$$\tau(E) = \hbar \frac{\partial \arg\{\mathfrak{T}(E)\}}{\partial E} \quad (1)$$

where  $\mathfrak{T}$  is the transition amplitude for photoionisation, and in the following discussions in this article, unless otherwise stated, we use the atomic units, where  $e = m_e = \hbar = 1$ , and the atomic unit of time 1 a.u.  $\approx 2.42 \times 10^{-17}$  s = 24.2 as. Although this definition is rather straightforward, and the transition amplitudes (phases and moduli) of one-photon ionisation for atoms and molecules can be routinely calculated by e.g. random-phase approximation with exchange (RPAE) [15, 16], time-dependent local-density approximation (TDLDA) [17, 18] and Schwinger variational methods such as ePolyScat [19, 20], in reality, the schemes of the phase measurements involves two-photon transitions, which differs from one-photon ionisation. An illustration of the RABBIT measurement scheme is illustrated in figure 1. The attosecond pulse train (APT) created by HHG contains typically odd harmonics of the fundamental driving field ( $\omega$ ), which leads to the main bands (dashed lines in figure 1). If a copy of the driving field is spatially and temporally overlapped with the APT as the dressing field, an additional sideband (solid line in figure 1) lying between the two main bands appears, which corresponds to either absorbing one photon from the lower main band (the absorption pathway), or emitting one photon from the higher main band (the emission pathway). The transition amplitudes of the absorption and the emission pathways can be written as:

$$\mathcal{A}_{\mp}(\Delta t) = \mathcal{A}_{\mp,0} \exp(\pm i\omega\Delta t) \quad (2)$$

where  $(-)$  and  $(+)$  in the subscript are for the absorption and the emission pathways, respectively. The relative time delay of the dressing field is denoted by  $\Delta t$  (the dressing field has the light path  $c\Delta t$  longer than the attosecond pulse, where  $c$  is the speed of light), meaning that at the time of the attosecond pulse burst the dressing field has the phase of  $\omega\Delta t$ . The transition amplitudes at  $\Delta t = 0$  are denoted as  $\mathcal{A}_{\mp,0}$ . The phase of

the dressing field contributes to the absorption and the emission pathways oppositely, and the side-band intensity is expressed by:

$$\mathcal{S}(\Delta t) = |\mathcal{A}_{\text{abs}} e^{i\omega\Delta t} + \mathcal{A}_{\text{emi}} e^{-i\omega\Delta t}|^2 = |\mathcal{A}_{\text{abs}}|^2 + |\mathcal{A}_{\text{emi}}|^2 + 2|\mathcal{A}_{\text{abs}}\mathcal{A}_{\text{emi}}| \cos(2\omega\Delta t - \phi) \quad (3)$$

where  $\phi = \arg\{\mathcal{A}_{\text{emi}}\} - \arg\{\mathcal{A}_{\text{abs}}\}$  is the phase difference between the emission and the absorption pathways. We can further write

$$\frac{\phi}{2\omega} = \tau_{\text{XUV}} + \tau_{\text{A}} \quad (4)$$

where  $\tau_{\text{XUV}} = (\phi_+^{\text{XUV}} - \phi_-^{\text{XUV}})/(2\omega)$  corresponds to the relative phase between the harmonic frequencies in the attosecond pulse, also known as the attochirp, and  $\tau_{\text{A}} = (\arg\{\mathfrak{T}_{\text{emi}}^{(2\text{ph})}\} - \arg\{\mathfrak{T}_{\text{abs}}^{(2\text{ph})}\})/(2\omega)$  is known as the two-photon ionisation time, since it corresponds to the phase difference of the two-photon transition amplitudes between the emission and the absorption pathways. More discussions and examples can be found in the book chapter [21].

From the theoretical point of view, the *ab initio* computation such as numerically solving the time-dependent Schrödinger equation (TDSE) is limited to the modelled potential with one active electron, e.g. the hydrogen-like atoms, while modelling the potential for molecules can be very challenging. A common approach for handling this problem is to separate the two-photon transition into two parts, i.e. the bound-continuum transition and the continuum-continuum transition, so that the two parts can be treated individually. This essentially stems from the lowest-order perturbation theory. The two-photon transition matrix element from an bound initial state  $|n\rangle$  to a final state in the continuum with momentum  $\vec{k}$  can be represented as [22]:

$$\mathcal{M}_n(\vec{k}'; \Omega) = \frac{1}{i} \lim_{\varepsilon \rightarrow 0^+} \mathfrak{F}_{\nu} \frac{\langle \vec{k}' | \hat{d}_{\omega} | \nu \rangle \langle \nu | \hat{d}_{\Omega} | n \rangle}{\varepsilon_n + \Omega - \varepsilon_{\nu} + i\varepsilon} \quad (5)$$

and the two-photon transition amplitude reads

$$\mathfrak{T}_{n \rightarrow l', m'}^{(2\text{ph})}(E'; \theta, \varphi) = \mathcal{E}_{\omega} \mathcal{E}_{\Omega} \mathcal{M}_n(\vec{k}'; \Omega) \quad (6)$$

where  $\mathcal{E}_{\Omega}$  and  $\mathcal{E}_{\omega}$  are the complex amplitudes (field strengths with phases included) of the XUV and dressing fields, respectively, and  $\vec{k}'$  is the vector with modulus of  $\sqrt{2E'}$  and pointing towards the emission angle  $(\theta, \varphi)$ , either in the lab frame or in the molecular frame for molecules. Within the framework of dipole approximation, the dipole terms for the XUV and dressing fields are  $\hat{d}_{\Omega}$  and  $\hat{d}_{\omega}$ , respectively. The  $\mathfrak{F}_{\nu}$  sign refers to summing over all discrete states and integrating over all continuous states. If one assumes that the two-photon process is dominated by the pathway that the electron absorbs one XUV photon from the initial state to an intermediate state in the continuum (assuming that the XUV photon energy is higher than the photoionisation energy) with the corresponding kinetic energy, after which a continuum-continuum transition occurs due to the presence of the dressing IR field, where the electron either absorbs or emits one IR photon (multi-IR processes are ignored here, assuming the dressing field is

relatively weak), as sketched in figure 1, then the two-photon transition amplitude can be expressed as:

$$\mathfrak{T}_{n \rightarrow l', m'}^{(2\text{ph})}(E') = \sum_{l, m} \mathfrak{T}_{n \rightarrow l, m}^{(1\text{ph})}(E) \mathfrak{T}_{l, m \rightarrow l', m'}^{(\text{CC})}(E, E') \quad (7)$$

where the terms  $\mathfrak{T}^{(1\text{ph})}(E)$  and  $\mathfrak{T}^{(\text{CC})}(E, E')$  refer to the bound-continuum and continuum-continuum transitions, respectively. Here we have decomposed the emission-angle-dependent transition amplitude into the spherical harmonics, i.e.

$$\mathfrak{T}_n^{(2\text{ph})}(E'; \theta, \varphi) = \sum_{l', m'} \mathfrak{T}_{n \rightarrow l', m'}^{(2\text{ph})}(E') Y_{l'}^{m'}(\theta, \varphi) \quad (8)$$

where  $Y_{l'}^{m'}(\theta, \varphi)$  is the spherical harmonic (in the Condon–Shortley phase convention) with angular momentum and magnetic quantum number of  $l'$  and  $m'$ , respectively. For the continuum-continuum part, the transition amplitude can be expressed as the product of the angular part and the radial part:

$$\mathfrak{T}_{l, m \rightarrow l', m'}^{(\text{CC})}(E, E') = \mathcal{E}_\omega \int_{4\pi} (Y_{l'}^{m'})^* Y_1^\mu Y_l^m d\Omega \times (-\pi) \int_0^\infty (R_{l'}(E))^* r R_l(E) r^2 dr \quad (9)$$

where  $Y_1^\mu$  is the polarisation of the dressing photon represented in the spherical harmonics. The  $(-\pi)$ -factor originates from the contour integral around the pole in equation (5), which is explained in detail in [22]. The angular part can be calculated by the Clebsch–Gordan coefficients:

$$\int_{4\pi} (Y_{l'}^{m'})^* Y_1^\mu Y_l^m d\Omega = \sqrt{\frac{3(2l+1)}{4\pi(2l'+1)}} \langle l, 0, 1, 0 | l', 0 \rangle \langle l, m, 1, \mu | l', m' \rangle \quad (10)$$

where  $\langle j_1, m_1, j_2, m_2 | J, M \rangle$  is the Clebsch–Gordan coefficient and is real in the Condon–Shortley phase convention. The latter integral between the radial wavefunctions, with the  $(-\pi)$ -term included, is denoted as  $\mathcal{T}_{l \rightarrow l'}(k, k')$  in the following discussion, where  $k = \sqrt{2E}$  and  $k' = \sqrt{2E'}$  are the momenta of the intermediate and final states, respectively. The radial wavefunctions in principle depend on the shape of the radial potential, which can be complicated for molecular cases. If we assume that the continuum-continuum transition is dominated by the long-range effect and is not sensitive to the local potential, then we can use the transition amplitudes derived from the hydrogen-like atoms. Therefore, instead of expression (1), the two-photon Wigner-like time delay is defined using the finite-difference method:

$$\tau^{(2\text{ph})}(E') = \frac{1}{2\omega} \left[ \arg\{\mathfrak{T}_{\text{emi}}^{(2\text{ph})}(E')\} - \arg\{\mathfrak{T}_{\text{abs}}^{(2\text{ph})}(E')\} \right] \quad (11)$$

which can be represented either in the spherical-coordinate basis  $(\theta, \varphi)$  or in the spherical-harmonic  $(l, m)$  basis. If we further assume that the continuum-continuum transition amplitude in equation (7) does not depend on  $(l, m)$  or  $(l', m')$ , then the

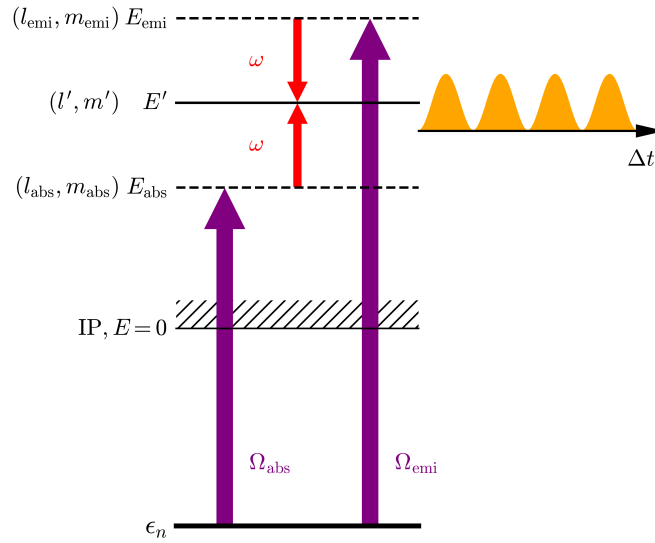


**Figure 1.** Typical energy diagram of the RABBIT scheme. The electron is excited from the bound initial state with  $\epsilon_n < 0$  with two frequency components  $\Omega_{\text{abs}}$  and  $\Omega_{\text{emi}}$  of the attosecond pulse train (purple arrows) to the corresponding intermediate states (dashed lines) with electron kinetic energies of  $E_{\text{abs}}$  and  $E_{\text{emi}}$ , respectively. The presence of the dressing field (red arrows) with frequency  $\omega$  induces the continuum-continuum transition from the intermediate states to the final state (sideband) with electron kinetic energy of  $E'$  and leads to the oscillation intensity of the sideband as a function of the XUV-IR time delay  $\Delta t$ , as sketched by the orange wave. The partial-wave indices are denoted as  $(l, m)$  for all states in the continuum, and the total transition amplitude is the superposition of the contributions from all possible pathways.

two-photon time delay can be separated into two parts:

$$\begin{aligned}
 \tau^{(2\text{ph})}(E') &= \frac{1}{2\omega} \left[ \arg\{\mathfrak{T}^{(1\text{ph})}(E_{\text{emi}})\mathfrak{T}^{(\text{CC})}(E_{\text{emi}}, E')\} - \arg\{\mathfrak{T}^{(1\text{ph})}(E_{\text{abs}})\mathfrak{T}^{(\text{CC})}(E_{\text{abs}}, E')\} \right] \\
 &= \frac{1}{2\omega} \left\{ \left[ \arg\{\mathfrak{T}^{(1\text{ph})}(E_{\text{emi}})\} - \arg\{\mathfrak{T}^{(1\text{ph})}(E_{\text{abs}})\} \right] \right. \\
 &\quad \left. + \left[ \arg\{\mathfrak{T}^{(\text{CC})}(E_{\text{emi}}, E')\} - \arg\{\mathfrak{T}^{(\text{CC})}(E_{\text{abs}}, E')\} \right] \right\} \\
 &\approx \tau^{(1\text{ph})}(E') + \tau_{\text{CC}}(E'; \omega)
 \end{aligned} \tag{12}$$

where we have approximated the derivative in expression (1) by its finite difference, and the continuum-continuum time delay is defined as

$$\tau_{\text{CC}}(E'; \omega) = \frac{1}{2\omega} \left[ \arg\{\mathfrak{T}^{(\text{CC})}(E_{\text{emi}}, E')\} - \arg\{\mathfrak{T}^{(\text{CC})}(E_{\text{abs}}, E')\} \right]. \tag{13}$$

By separating the two-photon time delay into the one-photon part and the continuum-continuum part, the problem is thus simplified as how to calculate the term  $\mathfrak{T}^{(\text{CC})}(E, E')$ , or equivalently the integral  $\mathcal{T}(k, k')$  for the hydrogen-like atoms. Dahlström *et al.* reported two models based on the Wentzel–Kramers–Brillouin (WKB) approximation with asymptotic expansion, i.e. considering the phase modulation (P) and considering

the phase and amplitude (modulus) modulation (P+A), both expressed by the analytical formulae involving the gamma function [23]:

$$\mathcal{T}_{\text{asym}}^{(\text{P})}(k, k') = \frac{\pi N_k N_{k'}}{2 |k - k'|^2} \exp \left[ -\frac{\pi Z}{2} \left( \frac{1}{k} - \frac{1}{k'} \right) \right] \frac{(2k)^{iZ/k} \Gamma[2 + iZ(1/k - 1/k')]}{(2k')^{iZ/k'} (k - k')^{iZ(1/k - 1/k')}} \quad (14)$$

and

$$\mathcal{T}_{\text{asym}}^{(\text{P+A})}(k, k') = \mathcal{T}_{\text{asym}}^{(\text{P})}(k, k') \left[ 1 + \frac{iZ}{2} \left( \frac{1}{k^2} + \frac{1}{k'^2} \right) \frac{k - k'}{1 + iZ(1/k + 1/k')} \right] \quad (15)$$

where  $N_k = \sqrt{2/(\pi k)}$  and  $N_{k'} = \sqrt{2/(\pi k')}$  are the normalisation factors for the intermediate state and the final state, respectively. We note that the normalisation factor depends on normalising according to the cross section or normalising according to the flux. Since for the scattered wave the total flux is

$$\int_{4\pi} j_s r^2 d\Omega = k \int_{4\pi} |f_s|^2 d\Omega = k \int_{4\pi} \frac{d\sigma}{d\Omega} d\Omega \quad (16)$$

where  $j_s$  is the scattering flux density,  $f_s$  is the scattering amplitude, and  $d\sigma/d\Omega$  is the differential cross section. The well-known solutions to the Coulomb wave equation are conventionally normalised according to the cross section, while the WKB approximation yields the flux-based normalisation factor, which contains an additional factor  $\propto k^{-1/2}$ , which is clear from comparing their asymptotic oscillation moduli [24]. The TDSE results lie typically between these two models, and they converge towards the same values for high kinetic energies [23]. A number of works have explicitly [11, 25, 26, 27, 28, 29, 30] or implicitly (e.g. to assume the two-photon time-delay difference between two species with the same or similar electron kinetic energies is equal or almost equal to their one-photon time-delay difference) [31, 32] used this assumption and have shown good agreement with the experimental results on molecules, indicating that this approximation is reasonable.

Despite the great success of this elegant model in the past decade, some features of experimental observations cannot be explained by these models. For example, the phases of these models do not depend on the angular momentum  $l$  of the intermediate or the final state, which causes that the angle-dependent time delay of two-photon ionisation is simply the angle-dependent time delay of one-photon ionisation plus an isotropic continuum-continuum time delay. This can be proven as follows. Using equations (7,9), we find

$$\mathfrak{T}_{n \rightarrow l', m'}^{(2\text{ph})}(E') = \mathcal{E}_\omega \sum_{l, m} \mathfrak{T}_{n \rightarrow l, m}^{(1\text{ph})}(E) \mathcal{T}_{\text{asym}}(\sqrt{2E}, \sqrt{2E'}) \int_{4\pi} (Y_{l'}^{m'})^* Y_1^\mu Y_l^m d\Omega. \quad (17)$$

Writing this formula into the spherical coordinates using equation (8), we have

$$\begin{aligned}
\mathfrak{T}_n^{(2\text{ph})}(E'; \theta', \varphi') &= \mathcal{E}_\omega \mathcal{T}_{\text{asym}}(\sqrt{2E}, \sqrt{2E'}) \int_{4\pi} \sum_{l', m'} Y_{l'}^{m'}(\theta', \varphi') \sum_{l, m} \mathfrak{T}_n^{(1\text{ph})}(E; \theta, \varphi) (Y_l^m(\theta, \varphi))^* \\
&\quad \times (Y_{l'}^{m'}(\tilde{\theta}, \tilde{\varphi}))^* Y_1^\mu(\tilde{\theta}, \tilde{\varphi}) Y_l^m(\tilde{\theta}, \tilde{\varphi}) \, d\tilde{\Omega} \\
&= \mathcal{E}_\omega \mathcal{T}_{\text{asym}}(\sqrt{2E}, \sqrt{2E'}) \int_{4\pi} \delta(\theta', \varphi'; \tilde{\theta}, \tilde{\varphi}) \delta(\theta, \varphi; \tilde{\theta}, \tilde{\varphi}) \\
&\quad \times Y_1^\mu(\tilde{\theta}, \tilde{\varphi}) \mathfrak{T}_n^{(1\text{ph})}(E; \theta, \varphi) \, d\tilde{\Omega} \\
&= \mathcal{E}_\omega \mathcal{T}_{\text{asym}}(\sqrt{2E}, \sqrt{2E'}) Y_1^\mu(\theta', \varphi') \mathfrak{T}_n^{(1\text{ph})}(E; \theta', \varphi') \tag{18}
\end{aligned}$$

where the term  $Y_1^\mu(\theta', \varphi')$  depends on the polarisation of the dressing field and does not contribute to the energy-dependent phase variation, i.e. the time delay. Hence, for helium one would expect an isotropic two-photon time delay, since its one-photon ionisation time delay has no angular dependence. This contradicts the experimental observation [33], and the mechanism was demonstrated in [34] that the moduli of the transition amplitudes for  $l \rightarrow l-1$  and  $l \rightarrow l+1$  have preference depending on the increase or decrease of the electron kinetic energy, which is known as the Fano's propensity rule in the continuum-continuum transition. The same mechanism was also confirmed by a more recent experimental work from the authors [35] using the circular-XUV-circular-IR RABBIT, where the Fano's propensity rule is embodied by the angle-dependent RABBIT phase difference between the co- and counter-rotating XUV and IR.

The missing piece was partially filled by Boll *et al.* who replaced the final-state wavefunction from the asymptotic formula by the regular solution of the Coulomb wave equation, which is expressed by the Kummer's function, or the confluent hypergeometric function of the first kind  ${}_1F_1$ . The result can also be written as an analytical expression using Gauss' hypergeometric function  ${}_2F_1$  [36]. This model quantitatively reproduces Fano's propensity rule at high electron kinetic energies and the angle-resolved time delay of helium [36, 37]. However, the agreement deteriorates at lower energies (typically below 10 eV), particularly for larger  $l$ 's, and in the same energy range the isotropic formulae proposed by Dahlström *et al.* also show large discrepancy compared to the TDSE. On the other hand, a lot of interesting phenomena in time delays, including shape resonance [30] and two-center interference [32] have been experimentally studied in this energy region, where the level of accuracy of the theory is partially limited by the reduced capability of the continuum-continuum delay models describing the relatively slow electrons. The general method for obtaining the  $N$ -photon transition amplitude from the  $(N-1)$ -photon transition amplitude has been known for a long time [38, 39], which involves expressing the Green's function by the Sturmian expansion and extending into the continuum. We shall show its application as a modification of expression (5). We give its analytical expression using the Appell's  $F_1$  function, which quantitatively agrees with the TDSE and the experimental results in the whole energy range including the low-kinetic-energy region. We also note that the isotropic model can be extended to the  $l$ -dependent model by expanding the WKB approximation to the next term, and the Fano's propensity rule and the  $l$ -dependent continuum-continuum transition phases

can be nicely reproduced.

This article is structured as following. In section 2, we first define the functions for the intermediate and final states, then we derive the analytical formula for the transition amplitudes between the Tricomi's and Kummer's functions. In section 3, we show multiple results including the continuum-continuum transition phases and time delays, and the Fano's propensity rule. These results are compared to TDSE and other theoretical approaches. We also compare our method to the experiment of circular-XUV-circular-IR RABBIT on helium [35]. The conclusion and outlook can be found in section 4.

## 2. Method

### 2.1. Regular and irregular solutions to the Coulomb wave equation

The radial Coulomb electronic wave equation for the hydrogen atom (central charge  $Z = 1$ ) with asymptotic kinetic energy  $E > 0$  and angular momentum  $l = 0, 1, 2, \dots$  reads (see [40], section (33.14) and [41], whereby equation (2) needs to be multiplied with  $(-1)$  for describing an attractive potential):

$$\frac{d^2 w}{dr^2} + \left( 2E + \frac{2}{r} - \frac{l(l+1)}{r^2} \right) w = 0 \quad (19)$$

where  $R(r) = w(r)/r$  is the radial wavefunction. Equation (19) can be adapted for arbitrary  $Z > 0$  by transforming  $\tilde{E} = Z^2 E$  and  $\tilde{r} = r/Z$ , where  $\tilde{E}$  and  $\tilde{r}$  are the asymptotic kinetic energy and the radius, respectively. For simplicity, in the discussion below we let  $Z = 1$ , while the treatment is general for any  $Z > 0$ . The regular solution of the outgoing radial wavefunction that satisfies the Coulomb wave equation can be written as (note that we have absorbed the factor  $k^{l+1}$  into  $C_l(k)$ , compared to the definition in [41]):

$$R_{k,l}^{\text{reg}}(r) \equiv f_l(k, r) = |C_l(k)| r^l \exp(ikr) \Phi(l+1-i/k, 2l+2, -2ikr) \quad (20)$$

where  $k = \sqrt{2E}$  is the momentum, and  $\Phi$  is the confluent hypergeometric function (Kummer's function), also known as the  ${}_1F_1$  function. Note that  $f_l(k, r)$  is a real function under such definition. The normalisation factor for the regular solution of the Coulomb wave equation with the Coulomb phase included is expressed as:

$$C_l(k) = k^{l+1} 2^l e^{\pi/(2k)} \frac{\Gamma(l+1+i/k)}{(2l+1)!} \quad (21)$$

such that  $r f_l(k, r)$  oscillates with amplitude of 1 at  $r \rightarrow \infty$ . Since equation (19) is a second-order differential equation, it has two linearly-independent solutions, and the other one can be expressed using the confluent hypergeometric function of the second kind  $U(a, b; z)$ , also known as the Tricomi's function:

$$u_l(k, r) = B_l(k) |C_l(k)| r^l \exp(ikr) U(l+1-i/k, 2l+2, -2ikr), \quad (22)$$

where we define the prefactor  $B_l(k)$  as:

$$B_l(k) = -2ie^{-\pi/k} (-1)^l \frac{(2l+1)!}{\Gamma(l+1+i/k)} \quad (23)$$



such that

$$f_l(k, r) = \Im\{u_l(k, r)\}. \quad (24)$$

Its real part is another real function that satisfies the Coulomb wave equation, also known as the irregular solution:

$$R_{k,l}^{\text{irr}}(r) \equiv g_l(k, r) = \Re\{u_l(k, r)\}. \quad (25)$$

We note that  $f_l(k, r)$  and  $g_l(k, r)$  are linear combinations of  $u_l(k, r)$  and its complex conjugate  $u_l^*(k, r)$ , which are two linearly independent solutions. Asymptotically,  $u_l(k, r)$  approaches the spherical wave with a position-dependent phase (the Coulomb phase) [41]:

$$\begin{aligned} u_l(k, r \rightarrow \infty) &= g_l(k, r \rightarrow \infty) + i f_l(k, r \rightarrow \infty) \\ &\approx (-i)^l \frac{1}{r} \exp\left(ikr + \frac{i}{k} \ln(2kr) - i \arg\{C_l(k)\}\right). \end{aligned} \quad (26)$$

Near the origin, the regular solution  $f_l(k, r) \sim r^l$  approaches zero, while the irregular solution  $g_l(k, r) \sim 1/r^{l+1}$  diverges. Although the irregular solution has infinitely large probability density near the origin, the product  $r^2 f_l(k, r) g_{l\mp 1}(k, r) \sim r^{1\pm 1}$  does not diverge near the origin, as plotted in figure 2 (note that the normalisation for Coulomb waves here ensures that  $rR(r)$  oscillates with modulus of 1 asymptotically), so the integral  $\int_0^{R_{\text{max}} > 0} f_l(k, r) r g_{l\mp 1}(k, r) r^2 dr$  is finite. In the framework of the Green's function method, the two photon ionisation amplitude is proportional to the following integral [42]:

$$\mathcal{I}_{l', l, \tilde{l}}^+ = \int_0^\infty dr \int_0^\infty d\tilde{r} R_{k', l'}(r) r^2 \mathfrak{g}_l^+(r, \tilde{r}; E) \tilde{r}^2 R_{\tilde{n}, \tilde{l}}(\tilde{r}) \quad (27)$$

where  $R_{\tilde{n}, \tilde{l}}(\tilde{r})$  and  $R_{k', l'}(r)$  are the radial wavefunctions of the initial (bound) and final (continuum) states, respectively, and  $\mathfrak{g}_l^+(r, \tilde{r}; E)$  is the Green's function of the intermediate state that couples the initial and the final states. For the Coulomb potential, the initial and final states are the regular solutions to the Coulomb equation. The radial Green's function in the three-dimensional space is [43, 44, 45]:

$$\mathfrak{g}_l^+(r, \tilde{r}; E) = \frac{\Gamma(l+1-i/k)}{2ikr_{>}r_{<}} W_{i/k; l+1/2}(-2ikr_{>}) \mathfrak{M}_{i/k; l+1/2}(-2ikr_{<}) \quad (28)$$

where  $k = \sqrt{2E}$  and  $r_{<} (r_{>})$  is the smaller (greater) variable between  $r$  and  $\tilde{r}$ . The Whittaker's functions  $\mathfrak{M}_{\kappa; \mu}(z)$  and  $W_{\kappa; \mu}(z)$  are related to the confluent hypergeometric functions by [40], section (13.14)

$$\mathfrak{M}_{\kappa; \mu}(z) = e^{-z/2} z^{\mu+1/2} \Phi(\mu+1/2-\kappa, 2\mu+1, z) \quad (29)$$

and

$$W_{\kappa; \mu}(z) = e^{-z/2} z^{\mu+1/2} U(\mu+1/2-\kappa, 2\mu+1, z). \quad (30)$$

If we assume that the bound-continuum transition occurs mainly in the short range due to the finite spatial extension of the initial wavefunction, and the continuum-continuum

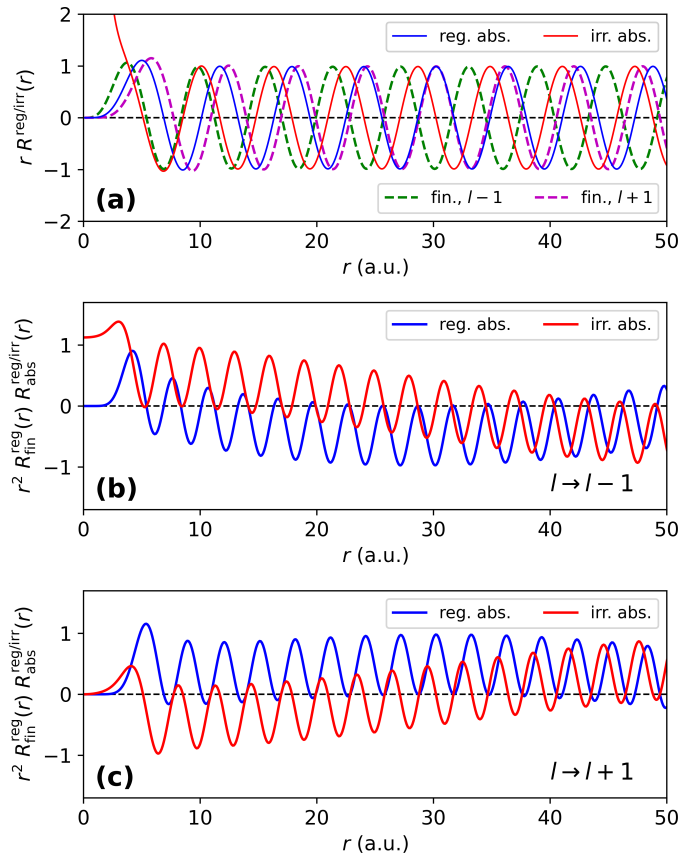


**Figure 2.** (a) Radial wavefunctions (without the phase factors) of the final states (fin., dashed) at  $E' = 15.00$  eV with  $l' = 3$  (green) or  $l' = 5$  (magenta), respectively, and the intermediate state of the absorption pathway (abs., solid) at  $E = 13.45$  eV with  $l = 4$ , where the photon energy of the dressing field is 1.55 eV. The regular (reg.) and irregular (irr.) parts of the intermediate state are plotted, while the final state has solely the regular part. (b) Products of the final-state radial wavefunction ( $l' = 3$ ) with the regular and the irregular parts of the intermediate-state radial wavefunction shown in (a), respectively. (c) The same as (b) but with the final state of  $l' = 5$ .

transition has major contribution from long range, we can replace  $r_>$  and  $r_<$  in the integral (27) by  $r$  and  $\tilde{r}$ , respectively. Thus, the two-photon transition amplitude is proportional to the product of

$$\mathcal{I}_{l,\tilde{l}} = \int_0^\infty f_l(k, \tilde{r}) \tilde{r} R_{\tilde{n},\tilde{l}}(\tilde{r}) \tilde{r}^2 d\tilde{r} \quad (31)$$

and

$$\mathcal{I}_{l',l}^+ = \int_0^\infty f_{l'}(k', r) r u_l(k, r) r^2 dr \quad (32)$$

which corresponds to the bound-continuum and continuum-continuum transitions, respectively. Note that the additional term  $r$  ( $\tilde{r}$ ) comes from the transform from the Whittaker's functions to the confluent hypergeometric functions. Therefore, equation

(5) is slightly modified as:

$$\mathcal{M}_n(\vec{k}'; \Omega) = \frac{1}{i} \lim_{\varepsilon \rightarrow 0^+} \sum_{\nu} \frac{\langle \vec{k}' | \hat{d}_{\omega} | \nu^+ \rangle \langle \nu | \hat{d}_{\Omega} | n \rangle}{\varepsilon_n + \Omega - \varepsilon_{\nu} + i\varepsilon} \quad (33)$$

where for bound states  $|\nu^+\rangle = |\nu\rangle$  and for continuum states  $|\nu^+\rangle$  is the outgoing-wave solution corresponding to the standing-wave solution  $|\nu\rangle$ . The former relation is also indicated by the fact that the confluent hypergeometric functions of the first kind ( $\Phi$ ) and second kind ( $U$ ) truncate into the same associated Laguerre polynomials for the bound states. Compared to the approach of Boll *et al.* [36], integral (32) uses the intermediate of the outgoing-wave solution to the Coulomb wave equation instead of its asymptotic form, which is also used in Dahlström *et al.*'s approach [23]. Therefore, we propose the following calculating procedure that if the final state from one-photon ionisation has partial wave with angular momentum  $l$  and asymptotically approaches  $\frac{1}{r} \exp(ikr)$ , we choose the intermediate state as

$$\begin{aligned} \tilde{u}_l(k, r) &= i^l e^{i \arg\{C_l(k)\}} u_l(k, r) \\ &= i^l B_l(k) C_l(k) r^l \exp(ikr) U(l+1 - i/k, 2l+2, -2ikr) \end{aligned} \quad (34)$$

and the final state as

$$\begin{aligned} i \tilde{f}_{l'}(k', r) &= i^{l'} e^{i \arg\{C_{l'}(k')\}} i f_{l'}(k', r) \\ &= i^{l'+1} C_{l'}(k') r^{l'} \exp(ik'r) \Phi(l'+1 - i/k', 2l'+2, -2ik'r) \end{aligned} \quad (35)$$

where  $(l, k)$  and  $(l', k')$  are the angular and linear momenta for the intermediate state and the final state, respectively. For the RABBIT experiment, where a photon from the dressing field is either absorbed (absorption pathway) or emitted (emission pathway), the final kinetic energy is  $E' = k'^2/2 = E \pm_{\text{emission}}^{\text{absorption}} \omega$ , while  $l' = l \pm 1$  can have both signs for each pathway, unless restricted by the magnetic quantum number in circular fields. For example, for the  $1s$  electron in hydrogen, if a linearly polarised XUV photon ionises it to the  $Ep_0$  continuum state ( $z$ -axis defined as the polarisation direction), and the dressing field is co-linearly polarised, both absorption and emission pathways lead to the superposition of  $E's_0$  and  $E'd_0$  states as the final state; on the other hand, if it is ionised by a circularly polarised XUV photon and has  $Ep_{+1}$  as the intermediate state ( $z$ -axis defined as the light propagation direction), and the dressing field is also circular with co-rotating polarisation, then for the absorption pathway only  $E'd_{+2}$  is allowed, while the emission pathway leads to the superposition of the  $E's_0$  and  $E'd_0$  states. The dipole transition amplitude between the intermediate state and the final state is therefore  $\mathcal{E}_{\omega} \mathcal{T}_{l \rightarrow l'}(k, k')$ , and  $\mathcal{T}_{l \rightarrow l'}(k, k')$  reads:

$$\mathcal{T}_{l \rightarrow l'}(k, k') = -\pi N_k N_{k'} \int_0^{\infty} \frac{1}{i} \tilde{f}_{l'}^*(k', r) r \tilde{u}_l(k, r) r^2 dr \quad (36)$$

where  $N_k = \sqrt{2/(\pi k)}$  and  $N_{k'} = \sqrt{2/(\pi k')}$  are the flux-based normalisation factors. In the following sections, we derive an analytical expression of equation (36) and related integrals. We will also give a simpler approximation that describes the asymptotic behaviour with consideration of the centrifugal energy following the WKB approximation.

2.2. General expression of integral containing the product of the confluent hypergeometric functions of the first and the second kind

Using the definition of  $\tilde{f}_l(k', r)$  and  $\tilde{u}_l(k, r)$ , we can write equation (36) into:

$$\begin{aligned} \mathcal{T}_{l \rightarrow l'}(k, k') &= -\pi N_k N_{k'} i^{l-l'-1} B_l(k) C_l(k) C_{l'}^*(k') \\ &\times \lim_{Q_0 \rightarrow 0^+} \int_0^\infty \exp[(ik + ik' - Q_0)r] r^{l+l'+3} \\ &\times U(l+1 - i/k, 2l+2, -2ikr) \\ &\times \Phi(l'+1 - i/k', 2l'+2, -2ik'r) dr \end{aligned} \quad (37)$$

where  $Q_0$  is a small positive number that ensures the integral converges according to the Abel-Dirichlet test [46]. Note that we have used the fact that  $\exp(ikr) \times \Phi(l+1 - i/k, 2l+2, -2ikr)$  is real and equal to its complex conjugate. Although the similar integral involving two Kummer's functions has already been discussed by Gordon almost a century ago [47] and the more general case is known to have the analytical formulation using the Appell's functions [48, 49, 50], to the best of our knowledge, the formula for the integral involving the product of the confluent hypergeometric functions of the first and second kind has yet to be explicitly demonstrated. Here we derive the analytical expression following the spirit of Gordon [47]. Let us consider the integral with a more general form:

$$\mathcal{J}_\rho^\sigma(a, b, \lambda; n', \lambda'; Q) = \int_0^\infty e^{-Q\xi} \xi^{\rho+\sigma} U(a, b; \lambda\xi) \Phi(-n', \rho+1; \lambda'\xi) d\xi. \quad (38)$$

The confluent hypergeometric function of the second kind can be represented as:

$$U(a, b; z) = \frac{1}{\Gamma(a)} \int_0^\infty e^{-zt} t^{a-1} (t+1)^{b-a-1} dt \quad (39)$$

with the following recurrence relations [40], equation (13.3.10):

$$U(a, b; z) = \frac{1}{z} [(b-a-1)U(a, b-1; z) + U(a-1, b-1; z)]. \quad (40)$$

Using equation (40), we have the relation:

$$\begin{aligned} \mathcal{J}_\rho^\sigma(a, b, \lambda; n', \lambda'; Q) &= \frac{1}{k} [(b-a-1)\mathcal{J}_\rho^{\sigma-1}(a, b-1, \lambda; n', \lambda'; Q) \\ &+ \mathcal{J}_\rho^{\sigma-1}(a-1, b-1, \lambda; n', \lambda'; Q)]. \end{aligned} \quad (41)$$

For  $\sigma > 0$ , which is the case for the transition between two continuum states (from equation (37) we have  $l-l'+2 = \pm 1 + 2$ ), the integral finally comes to  $\sigma = 0$  terms:

$$\mathcal{J}_\rho^0(a, b, \lambda; n', \lambda'; Q) = \int_0^\infty e^{-Q\xi} \xi^\rho U(a, b; \lambda\xi) \Phi(-n', \rho+1; \lambda'\xi) d\xi. \quad (42)$$

In particular, we can write the two expressions for  $\sigma = 1$  and 3 explicitly:

$$\begin{aligned} \mathcal{J}_\rho^1(a, b, \lambda; n', \lambda'; Q) &= \frac{1}{k} [(b-a-1)\mathcal{J}_\rho^0(a, b-1, \lambda; n', \lambda'; Q) \\ &+ \mathcal{J}_\rho^0(a-1, b-1, \lambda; n', \lambda'; Q)] \end{aligned} \quad (43)$$

and

$$\begin{aligned} \mathcal{J}_\rho^3(a, b, \lambda; n', \lambda'; Q) &= \frac{1}{k^3} [(b-a-3)(b-a-2)(b-a-1)\mathcal{J}_\rho^0(a, b-3, \lambda; n', \lambda'; Q) \\ &\quad + 3(b-a-2)(b-a-1)\mathcal{J}_\rho^0(a-1, b-3, \lambda; n', \lambda'; Q) \\ &\quad + 3(b-a-1)\mathcal{J}_\rho^0(a-2, b-3, \lambda; n', \lambda'; Q) \\ &\quad + \mathcal{J}_\rho^0(a-3, b-3, \lambda; n', \lambda'; Q)]. \end{aligned} \quad (44)$$

In order to obtain  $\mathcal{J}_\rho^0(a, b, \lambda; n', \lambda'; Q)$ , we use equation (39), thus

$$\mathcal{J}_\rho^0(a, b, \lambda; n', \lambda'; Q) = \frac{1}{\Gamma(a)} \int_0^\infty \int_0^\infty e^{-(Q+\lambda t)\xi} t^{a-1} (t+1)^{b-a-1} \xi^\rho \Phi(-n', \rho+1; \lambda'\xi) dt d\xi. \quad (45)$$

By using the following formula for the  ${}_2F_1$  function [51], equation (07.23.07.0003.01):

$${}_2F_1(\alpha, \beta, \gamma; z) = \frac{1}{\Gamma(\beta)} \int_0^\infty e^{-\xi} \xi^{\beta-1} \Phi(\alpha, \gamma; \xi z) d\xi \quad (46)$$

and swapping the order of integration, we have:

$$\mathcal{J}_\rho^0(a, b, \lambda; n', \lambda'; Q) = \frac{\rho!}{\Gamma(a)} \int_0^\infty \frac{t^{a-1} (t+1)^{b-a-1}}{(Q+\lambda t)^{\rho+1}} {}_2F_1\left(-n', \rho+1, \rho+1, \frac{\lambda'}{Q+\lambda t}\right) dt. \quad (47)$$

Using the definition of the generalised hypergeometric functions [51], equation (07.19.02.0002.01):

$${}_2F_1(\alpha, \beta, \beta; z) = {}_1F_0(\alpha; ; z) = (1-z)^{-\alpha} \quad (48)$$

we have:

$$\begin{aligned} \mathcal{J}_\rho^0(a, b, \lambda; n', \lambda'; Q) &= \frac{\rho!}{\Gamma(a)} \int_0^\infty \frac{t^{a-1} (t+1)^{b-a-1}}{(Q+\lambda t)^{\rho+1}} \left(1 - \frac{\lambda'}{Q+\lambda t}\right)^{n'} dt \\ &= \frac{\rho! (Q-\lambda')^{n'}}{Q^{\rho+1+n'}} \int_0^\infty t^{a-1} (t+1)^{b-a-1} \left(\frac{\lambda}{Q}t+1\right)^{-(\rho+1+n')} \left(\frac{\lambda}{Q-\lambda'}t+1\right)^{n'} dt. \end{aligned} \quad (49)$$

Let us use the integral representation of the Appell's  $F_1$  function [51], equation (07.36.07.0001.01):

$$\begin{aligned} F_1(\alpha; \beta_1, \beta_2; \gamma; z_1, z_2) &= \frac{\Gamma(\gamma)}{\Gamma(\alpha)\Gamma(\gamma-\alpha)} \int_0^1 \frac{h^{\alpha-1} (1-h)^{\gamma-\alpha-1}}{(1-hz_1)^{\beta_1} (1-hz_2)^{\beta_2}} dh \\ &= \frac{\Gamma(\gamma)}{\Gamma(\alpha)\Gamma(\gamma-\alpha)} \int_0^\infty \frac{(t+1)^{\beta_1+\beta_2-\gamma} t^{\alpha-1}}{[(1-z_1)t+1]^{\beta_1} [(1-z_2)t+1]^{\beta_2}} dt \end{aligned} \quad (50)$$

where we used  $h = \frac{t}{t+1}$ . Compared to equation (49), we have  $\alpha = a$ ,  $\beta_1 = \rho+1+n'$ ,  $\beta_2 = -n'$ ,  $\gamma = \rho-b+a+2$ ,  $z_1 = 1 - \frac{\lambda}{Q}$ , and  $z_2 = 1 - \frac{\lambda}{Q-\lambda'}$ . Therefore, we finally get

$$\begin{aligned} \mathcal{J}_\rho^0(a, b, \lambda; n', \lambda'; Q) &= \frac{\Gamma(\rho-b+2)}{\Gamma(\rho-b+a+2)} \frac{\rho! (Q-\lambda')^{n'}}{Q^{\rho+1+n'}} \\ &\quad \times F_1\left(a; \rho+1+n', -n'; \rho-b+a+2; 1 - \frac{\lambda}{Q}, 1 - \frac{\lambda}{Q-\lambda'}\right) \\ &= \frac{\Gamma(\rho-b+2)}{\Gamma(\rho-b+a+2)} \frac{\rho!}{\lambda^{\rho+1}} \\ &\quad \times F_1\left(\rho-b+2; \rho+1+n', -n'; \rho-b+a+2; 1 - \frac{Q}{\lambda}, 1 - \frac{Q-\lambda'}{\lambda}\right) \end{aligned} \quad (51)$$

where in the last step we used the relation [52], equation (5.11.1):

$$F_1(\alpha; \beta_1, \beta_2; \gamma; z_1, z_2) = (1 - z_1)^{-\beta_1} (1 - z_2)^{-\beta_2} F_1\left(\gamma - \alpha; \beta_1, \beta_2; \gamma; \frac{z_1}{z_1 - 1}, \frac{z_2}{z_2 - 1}\right). \quad (52)$$

With help of equations (41, 43, 44), we can calculate the multipole transition amplitudes between states expressed by the confluent hypergeometric functions of the first and the second kind. Therefore, equation (37) can be expressed as: ‡

$$\begin{aligned} \mathcal{T}_{l \rightarrow l'}(k, k') &= -\pi N_k N_{k'} i^{l-l'-1} B_l(k) C_l(k) C_{l'}^*(k') \\ &\times \lim_{Q_0 \rightarrow 0^+} \mathcal{J}_{2l'+1}^{l-l'+2} \left( l + 1 - \frac{i}{k}, 2l + 2, -2ik; -\left( l' + 1 - \frac{i}{k'} \right), -2ik'; Q_0 - i(k + k') \right). \end{aligned} \quad (53)$$

One can find the similarity between our equations (41, 43, 44, 51) and the equation (3.1) in reference [50]. In fact, we can write

$$\begin{aligned} B_l(k) |C_l(k) C_{l'}(k')| \mathcal{J}_{2l'+1}^{l-l'+2} \left( l + 1 - \frac{i}{k}, 2l + 2, -2ik; -\left( l' + 1 - \frac{i}{k'} \right), -2ik'; Q_0 - i(k + k') \right) \\ = \int_0^\infty f_{l'}(k', r) r e^{-Q_0 r} u_l(k, r) r^2 dr \\ = \int_0^\infty f_{l'}(k', r) r e^{-Q_0 r} g_l(k, r) r^2 dr \\ + i \int_0^\infty f_{l'}(k', r) r e^{-Q_0 r} f_l(k, r) r^2 dr \end{aligned} \quad (54)$$

and one immediately sees that for the purpose of calculating the transition amplitude between two regular solutions to the Coulomb wave equation, also known as the Gordon's integral, the result is given by the imaginary part of equation (54), which is also given in [48, 49, 50], while its real part corresponds to the transition amplitude between the regular and irregular solutions, where the regular and irregular solutions are defined to be real functions. We note that our formula has similarity to the general expression for the double- or multi-photon ionisation amplitude from bound states of hydrogen atoms given in references [53, 54], which use the Sturman expansion with modifications in the continuum.

### 2.3. Asymptotic formula for the CC transition amplitude with the centrifugal potential included

The purpose of this section is to demonstrate the mechanism with simpler mathematical expressions. Such approaches are usually available for describing the asymptotic behaviour at high kinetic energies, while we try to make the compromise that the formula applied at low kinetic energies should at least give a qualitative description,

‡ Here we make a special note that although  $Q_0$  in equation (53) can be exactly zero, where the last two arguments in equation (51) are real and can be evaluated by analytic continuation when one of them has modulus greater than 1. However, due to the ambiguous phase of  $(-1)$  that occurs upon analytic continuation, one of the branches of the parameters may become incorrect, which means that taking the complex conjugates of all the first four arguments in  $F_1$  does not return the complex conjugate of the result, although from its definition one would expect so. Therefore, it is recommended to numerically confirm that the case of  $Q_0 = 0$  is indeed the limit of  $Q_0 = 0^+$ .

such that the main features are still captured. Let us consider the phase contribution of the centrifugal potential under the WKB approximation. The phase factor of the outgoing wave can be written as:

$$\begin{aligned}
S_l(k, r) &= \int_0^r \sqrt{\frac{2}{\mathfrak{r}} - \frac{2b}{\mathfrak{r}^2} + k^2} \, d\mathfrak{r} \\
&= \int_0^r k + \frac{\mathfrak{r}^{-1}}{k} - \frac{\mathfrak{r}^{-2}(2k^2b + 1)}{2k^3} + \mathcal{O}(\mathfrak{r}^{-3}) \, d\mathfrak{r} \\
&= kr + \ln(2kr)/k + r^{-1} \frac{2k^2b + 1}{2k^3} + \mathcal{O}(r^{-2})
\end{aligned} \tag{55}$$

where  $b = l(l+1)/2$  comes from the centrifugal potential, and the expansion is made at  $r \rightarrow \infty$ . Thus, the outgoing radial wave function can be estimated as:

$$\begin{aligned}
rR_{k,l}(r) &\approx \exp(iS_l(k, r)) \\
&= e^{ikr} (2kr)^{i/k} \exp(iqr^{-1} + \mathcal{O}(r^{-2})) \\
&= e^{ikr} (2kr)^{i/k} (1 + iqr^{-1} + \mathcal{O}(r^{-2}))
\end{aligned} \tag{56}$$

where  $q = (2k^2b + 1)/(2k^3)$  scales with  $k^{-3}$  for the  $s$  ( $l = 0$ ) wave, but with  $k^{-1}$  for waves with higher angular momenta. This explains why the phase contribution of the centrifugal potential should not be neglected, as  $k^{-1}$  is a rather slow convergence under the experimental context (typically  $E = 10^1 \sim 10^2$  eV,  $k = 1 \sim 3$  a.u.). The dipole transition between two outgoing waves can thus be approximated as:

$$\begin{aligned}
\mathcal{T}_{l \rightarrow l'}^{(P)}(k, k'; r_0) &\approx -\frac{\pi}{2} N_k N_{k'} \frac{(2k)^{i/k}}{(2k')^{i/k'}} \int_{r_0}^{\infty} e^{-i(k'-k)r} r^{i/k - i/k'} [r + i(q - q') + \mathcal{O}(r^{-1})] \, dr \\
&\approx -\frac{\pi}{2} N_k N_{k'} \frac{(2k)^{i/k}}{(2k')^{i/k'}} \left[ \frac{\Gamma(s, \Lambda r_0)}{\Lambda^s} + i(q - q') \frac{\Gamma(s-1, \Lambda r_0)}{\Lambda^{s-1}} \right]
\end{aligned} \tag{57}$$

where  $s = 2 + i/k - i/k'$  and  $\Lambda = i(k' - k)$ . The factor of  $1/2$  comes from the fact that the final state represented by the Kummer's function contains the  $k'$ - and  $(-k')$ -parts, while the  $(-k')$ -part practically vanishes due to the large imaginary part in the gamma function [55]. Here we have used the incomplete gamma function

$$\Gamma(s, x) = \int_x^{\infty} t^{s-1} e^{-t} \, dt \tag{58}$$

to include the case where the integral starts from  $r_0 > 0$  instead of 0. This can be useful for the more complex scattering problem, where the (time-dependent) Schrödinger equation is numerically solved inside the radius  $r_0$ , while the outgoing electron wavefunction is extrapolated beyond  $r_0$  using the  $l$ -dependent asymptotic formula, assuming that the potential is converged except the Coulomb ( $\sim \mathcal{O}(r^{-1})$ ) and centrifugal-like ( $\sim \mathcal{O}(r^{-2})$ ) parts. When  $r_0 = 0$ ,  $\Gamma(s, 0) = \Gamma(s)$  is the gamma function, and  $\Gamma(s)/\Gamma(s-1) = s-1$ . The first term in equation (57) corresponds to equation (14) reported by Dahlström *et al.* [22, 23, 56], and the second term depends on the angular momenta of the initial and the final states.

We note that Dahlström *et al.* also reported another formula (equation (15)) that has the correction for the amplitude factor according to the WKB approximation:

$$rR_{k,l}(r) \approx \exp(iS_l(k, r))k^{1/2}(2/r + k^2)^{-1/4} \quad (59)$$

where the amplitude factor is

$$\left(\frac{2}{k^2r} + 1\right)^{-1/4} = 1 - \frac{1}{2k^2r} + \mathcal{O}(r^{-2}). \quad (60)$$

Following the similar treatment, equation (57) is modified as

$$\mathcal{T}_{l \rightarrow l'}^{(P+A)}(k, k'; r_0) \approx -\frac{\pi}{2} N_k N_{k'} \frac{(2k)^{i/k}}{(2k')^{i/k'}} \left[ \frac{\Gamma(s, \Lambda r_0)}{\Lambda^s} + (iq - iq' - Q - Q') \frac{\Gamma(s-1, \Lambda r_0)}{\Lambda^{s-1}} \right] \quad (61)$$

where  $Q = 1/(2k^2)$ . The superscripts (P) and (P + A) in equations (57, 61) refer to including the phase variation and the phase and amplitude variations, respectively. For the hydrogen atom at low kinetic energies, the phase computed by TDSE typically lies between equation (57) and equation (61) with  $r_0 = 0$ . Although the agreement may improve by choosing a suitable  $r_0$  in a similar fashion as in the (P+A') model of reference [23], it is better to evaluate according to equation (53).

#### 2.4. Numerical evaluation

For numerical evaluation in this work, we used Python 3.8.10 [57] with numpy 1.20.2 [58] and mpmath 1.1.0 [59]. The latter package is capable of calculating many special functions with complex arguments.

### 3. Results and discussion

#### 3.1. Continuum-continuum transition phase for the hydrogen atom

In order to test the accuracy of the analytical formula and its asymptotic approximations, we compare to the time-dependent Schrödinger equation (TDSE) results reported in [23, 36], which are currently considered to be the benchmark for the CC transition amplitudes. As shown in figure 3, our equation (53) perfectly agrees with the TDSE values, which manifests the validity of our approach. Regarding the asymptotic approximations, the (P) and (P+A) formulae given by Dahlström *et al.* are independent of the angular momentum  $l'$  (isotropic), and the CC phases of  $p \rightarrow s$  and  $p \rightarrow d$  lie between the two approximations. The modified asymptotic approximation (P) given by equation (57) reproduces the phase difference between the  $p \rightarrow s$  and  $p \rightarrow d$  channels, indicating that the effect of the centrifugal potential is indeed captured by the expansion, although they both overestimate the absolute value of the phase at low kinetic energies, as in the case of the isotropic formula. On the other hand, the modified asymptotic approximation (P+A) given by equation (61) show very little difference between  $p \rightarrow s$  and  $p \rightarrow d$ , and both of them are well aligned with the corresponding



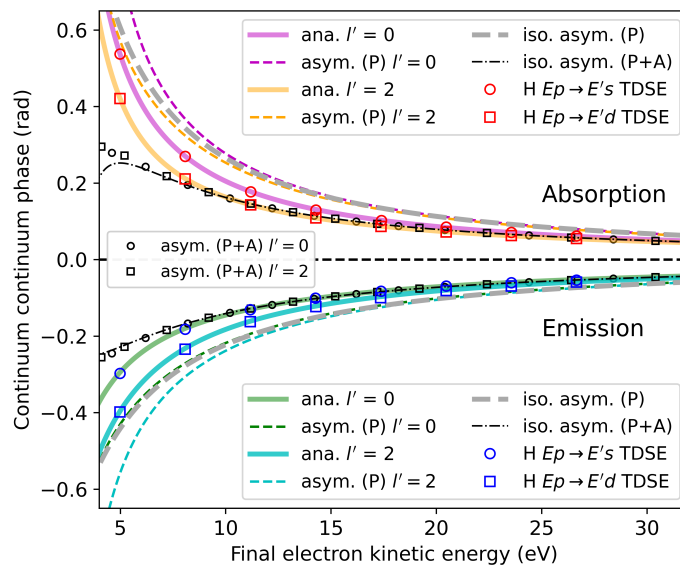


**Figure 3.** The phase of the CC transition (with dressing field wavelength of 800 nm) for the hydrogen atoms from the intermediate state of  $l = 1$  to the final state of  $l' = 1 \mp 1$ . The electron kinetic energy refers to the final state ( $E'$ ). The analytical formula (ana.) corresponds to (53); the  $l$ -dependent asymptotic approximation with phase correction (asym. (P),  $r_0 = 0$ ) corresponds to (57); the  $l$ -dependent asymptotic approximation with phase and amplitude correction (asym. (P+A),  $r_0 = 0$ ) corresponds to (61); the isotropic asymptotic approximation with phase correction (iso. asym. (P)) and with phase and amplitude correction (iso. asym. (P+A)) are taken from [23]; the TDSE results are taken from [36], which practically overlap with the SOPT calculation.

isotropic formula. This is because at low kinetic energies the amplitude-variation effect overrides the phase-variation effect, while the former is independent of  $l'$  under the far-field expansion up to  $\mathcal{O}(r^{-1})$ .

### 3.2. Fano's propensity rule in continuum-continuum transition

Fano's propensity rule in CC transition reported in references [34, 36] is tested using our equation (53) and its asymptotic approximations, as shown in figure 4. The analytical formula again shows excellent agreement with TDSE [23, 36], SOPT [60], and RPAE [34] for intermediate states with various angular momenta. We note that the modified asymptotic approximation shows very good agreement from about 15 eV, where the absorption pathway converges seemingly faster than the emission pathway. The (P) and (P+A) approximations ( $r_0 = 0$ ) give very similar moduli ratios, as the amplitude variation effect is mostly cancelled in the ratios. The Fano's propensity rule is entirely absent from the isotropic asymptotic formulae, since they do not have  $l$ -dependence. This indicates that the main effect from the centrifugal potential is well described by the expansion of the phase to the next order, which is a good approximation for  $k \gtrsim 1$  a.u..

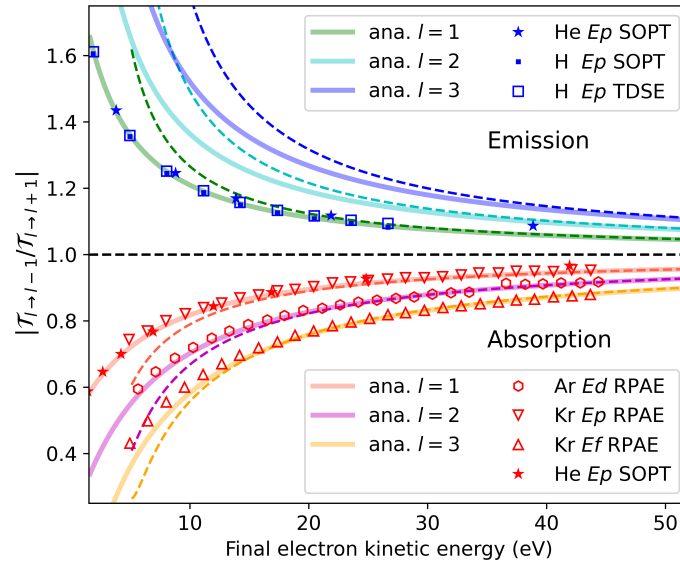


**Figure 4.** Moduli ratios for the absorption and emission pathways (with dressing field wavelength of 800 nm). The analytical formula (ana.) corresponds to (53) and the results are shown by the thick solid curves, while the results from the  $l$ -dependent asymptotic approximation (57,61) are shown by the thin dashed curves with the corresponding colours, where the results from the (P) and (P+A) formulae almost overlap, so only the ones from (P) are shown. The computational results (RPAE, SOPT, TDSE) are taken from [36], where the RPAE results originate from [34]. The angular momentum  $l$  corresponds to the intermediate state, while the electron kinetic energy corresponds to the final state.

### 3.3. Continuum-continuum transition time delay

The continuum-continuum transition time delay defined by the finite difference is

$$\tau_{CC}(E) = \frac{1}{2E_{CC}} \left( \phi^{\text{emi}}(E_+ \rightarrow E) - \phi^{\text{abs}}(E_- \rightarrow E) \right) \quad (62)$$

where  $E_{\pm} = E \pm E_{CC}$  is the electron kinetic energy of the intermediate state, and  $\phi$  is the phase of the transition amplitude. The results given by the analytical formula (53) are plotted in figure 5. The values for the  $Ep \rightarrow E's$  and  $Ep \rightarrow E'd$  channels agree perfectly with the TDSE for hydrogen atoms. The (P) and (P+A) formulae reported by Dahlström *et al.* [23] and with the modification introduced in this work lie below and above the curves, respectively. In particular, the (P+A) formula bends to the opposite direction at lower kinetic energies, although it matches the TDSE better at higher kinetic energies. This again manifests the validity of our analytical formula. Interestingly, although the phases of different  $l$ -channels vary, as shown in figure 3, the phase differences between the emission and absorption pathways ( $l \leq 3$ ) are very close, which has recently been reported by Busto *et al.* [21]. Hence, the key problem is to correctly determine the relative phase offset between channels and their moduli ratios, which can be accurately achieved by the analytical formula, as demonstrated in the

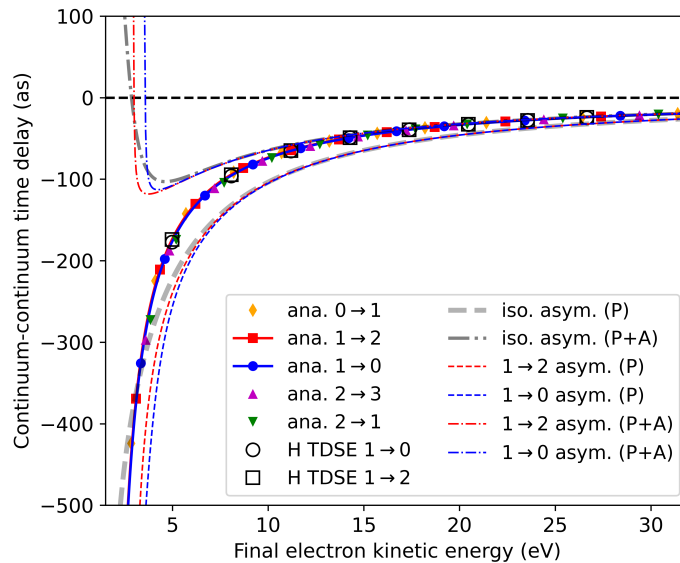


**Figure 5.** The CC time delays obtained from the phases shown in figure 3. The TDSE results from hydrogen atoms are taken from [36]; the isotropic asymptotic approximation are taken from [23]; the other markers and curves are given by the analytical formula (53) labelled as “(intermediate angular momentum)  $\rightarrow$  (final angular momentum)”. The electron kinetic energy corresponds to the final state.

previous sections.

#### 3.4. Angle-dependent time delay for helium with circular-XUV-circular-IR RABBIT

An experimental test for the angular-momentum-dependent continuum-continuum transition amplitude are angle-resolved time-delay measurements on atoms [61, 33, 62]. For example, using the (isotropic) asymptotic wavefunction for the intermediate state and the Kummer’s function for the final state [36], Boll *et al.* showed that this analytical formula with partial approximation matches well with the linear-XUV-linear-IR RABBIT experiments regarding the angle-dependent phase [37]. We note that due to the relatively large experimental uncertainties at emission angles close to  $90^\circ$ , where different theoretical models differ most, it is not obvious to decide which model is the most accurate, especially at lower electron kinetic energies. Here we compare the theories with a circular-XUV-circular-IR RABBIT experiment reported recently by the present authors [35]. The scheme for the generation and characterisation of the circular XUV attosecond pulse trains and the experimental setup for angle-resolved RABBIT have been described in our recent publications [35, 63, 64]. The benefit of the circular-XUV-circular-IR RABBIT scheme for helium is that the difference in the co- and counter-rotating XUV and IR provides additional information of the partial waves. For example, if the circular XUV excites one of the helium electrons from  $1s$  to the  $Ep_1$  intermediate state (the  $z$ -axis is defined as the light-propagation direction), in the

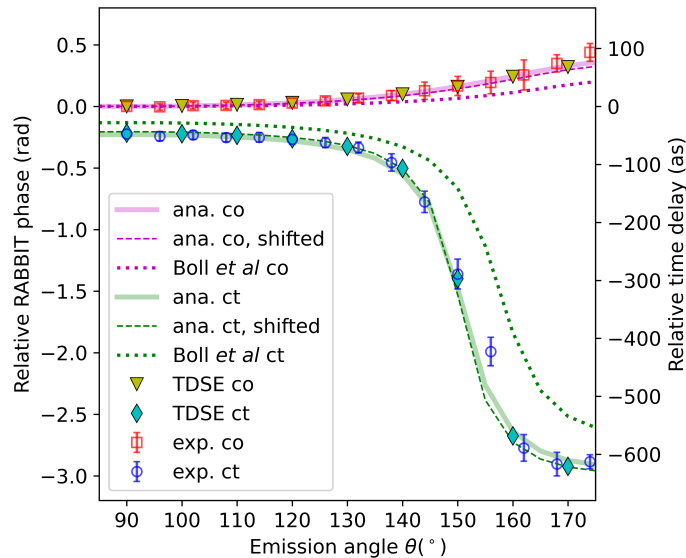


**Figure 6.** Angle-dependent RABBIT phases and corresponding relative time delays of helium for co-rotating (co) and counter-rotating (ct) XUV and dressing IR (800 nm) with final-state kinetic energy of 3.3 eV (SB18). The phases and relative time delays are referenced to the co-rotating case with electron emitted at  $90^\circ$ . The experimental (exp.) and TDSE values are reported in [35]. The analytical (ana.) results are obtained from (53), including the calculation using unshifted and shifted center of expansion by 1 Å, shown as the solid and dashed lines, respectively. The dotted lines correspond to the values calculated by the formula proposed by Boll *et al.* [36]. The one-photon ionisation amplitude is calculated using ePolyScat [19, 20].

continuum-continuum transition step, if the dressing field is co-rotating with the XUV, then the absorption pathway leads only to the  $E'd_2$  final state due to the restriction of the magnetic quantum number, while the emission pathway leads to the superposition of the  $E's$  and  $E'd_0$  states; on the contrary, if the dressing field is counter-rotating, then the emission pathway yields the  $E'd_2$  final state, and the absorption pathway gives the superposition of the  $E's$  and  $E'd_0$  states. Since there are only three partial waves contributing to a given sideband, their individual moduli and phases can be extracted by the global fitting of the two-dimensional interference pattern [65] with only six parameters. By comparing the co-rotating and counter-rotating cases, one can separate the Wigner part  $1s \rightarrow Ep$  and the continuum-continuum part  $Ep \rightarrow E's/d$  of the photoionisation time delays for each final state [35]. Theoretically, the angular dependence of the RABBIT phase is entirely absent from the isotropic asymptotic approximations, and the relative phase and modulus ratio between  $Ep \rightarrow E's$  and  $Ep \rightarrow E'd$  play the key role, as explained in [34]. The theoretical and experimental results are compared in figure 6. We choose SB18 with relatively low electron kinetic energy (3.3 eV), where the asymptotic formulae have poor accuracy and are not shown in the figure. Our proposed analytical formula (53) shows remarkably good agreement with the TDSE and experimental values for both the co- and counter-rotating cases, which is

expected from the level of accuracy that it has shown in describing the moduli and phases of the transition amplitudes between different  $l$ -states. The formula proposed by Boll *et al.* is known to have less accuracy at lower electron kinetic energies and agrees with the TDSE and experimental values semi-quantitatively. Considering the precision of the experimental values, we conclude that our analytical formula quantitatively reproduces the experimental results and has comparable accuracy with the TDSE computation, which outperforms the formula proposed by Boll *et al.* at low electron kinetic energies.

**Table 1.** Partial-wave fractions of helium one-photon ionisation with expansion center shifted by 1 Å, calculated using ePolyScat [19, 20].

$E_k$ (eV)	$l = 0$	$l = 1$	$l = 2$	$l = 3$	$l > 3$
3.3	0.0808	0.7484	0.1617	0.0088	0.0002
18.8	0.1891	0.2266	0.3970	0.1599	0.0274

In order to further check the sensitivity of our method regarding the shape of the potential, we performed calculations with helium one-photon photoionisation amplitudes with an expansion center displaced by 1 Å using ePolyScat [19, 20]. Since ePolyScat uses single-center expansions, when the atomic orbitals are displaced from the center of expansion, a series of (in principle infinite number of) partial waves are involved, in contrast to the centered helium atom, where the one-photon ionisation solely leads to the  $p$ -wave. The fractions (defined as the modulus square ratio) of partial waves of the shifted helium atom with electron kinetic energies of 3.3 eV and 18.8 eV are summarised in table 1. At 3.3 eV,  $l = 1$  ( $p$ -wave) is still dominating, with some contributions from  $l = 0$  and  $l = 2$  partial waves. As the electron kinetic energy increases to 18.8 eV, the distribution becomes more diffuse, with  $l = 2$  as the leading partial wave and comparable contributions from  $l = 0, 1, 3$ . Although all the observables at asymptotic distance from the origin should be insensitive to the shift of the atom, depending on the model, this may introduce artefacts. When the atom is displaced from the origin in the spherical coordinate, the potential is no longer central, and the unshifted Coulomb waves are no longer its eigenfunctions. On the other hand, one may argue that since the continuum-continuum transition involves the outgoing electron wavepackets that escape from the atom, the transition amplitude should be less sensitive to the short-range potential, and the asymptotic behaviour is the same. The results using the analytical formula for the lower kinetic energy (3.3 eV) are shown as the dashed lines in figure 6, where the phase difference compared to the unshifted case is only marginal. For the higher kinetic energy (18.8 eV), we compare the results using the analytical formula (53), the formula proposed by Boll *et al.* [36], and the modified asymptotic formula ((P), equation (57),  $r_0 = 0$ ) in figure 7. Since the electron kinetic energy is relatively high, all three models show reasonable agreement with the experimental values. For the shifted helium, the time delay from the modified asymptotic formula is practically unchanged, since it is by

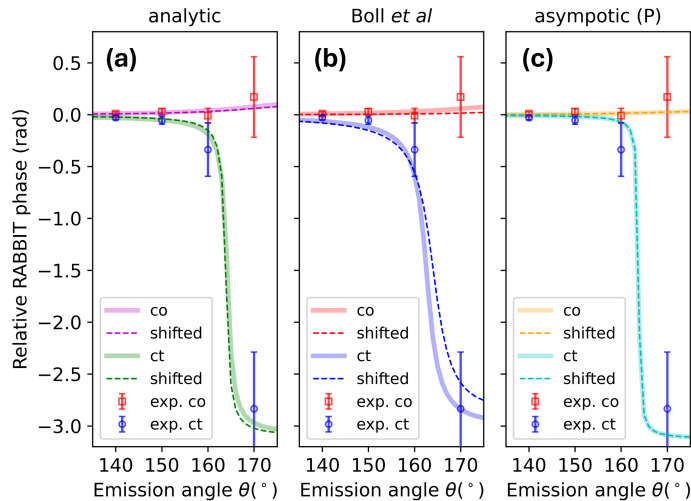


**Figure 7.** Angle-dependent RABBIT phases of helium for co-rotating (co) and counter-rotating (ct) XUV and dressing IR (800 nm) with final-state energy of 18.8 eV (SB28). The phases and relative time delays are referenced to the co-rotating case with electron emitted at  $90^\circ$ . Panel (a) uses the analytic formula in this work (53); panel (b) uses the formula proposed by Boll *et al.* [36]; panel (c) uses the modified asymptotic formula ((P), equation (57),  $r_0 = 0$ ). In all panels, the experimental (exp.) values are taken from [35]. The dashed lines with corresponding colours refer to the results of shifting the expansion center by  $1 \text{ \AA}$ . The one-photon ionisation amplitude is calculated using ePolyScat [19, 20].

its nature only sensitive to the asymptotic behaviour, whereas the formula proposed by Boll *et al.* shows a non-negligible phase difference, indicating that the time delay may be less accurate when the potential deviates from the perfect central potential. The analytical formula shows much smaller difference, which implies that although taking the confluent hypergeometric function of the second kind may deviate from the reality in a non-central potential field, e.g. the potential of a molecular cation, the calculated time delay is largely converged.

#### 4. Conclusion

In conclusion, we have proposed an analytical formula for calculating the continuum-continuum transition amplitudes for the hydrogen-like atoms which uses the confluent hypergeometric functions of the first and second kinds as the final and intermediate states, respectively. We first derived the integral between the confluent hypergeometric functions of the first and second kinds, which can be expressed using the Appell's  $F_1$  function. We note that this expression is an extension to the Gordon's integral, as the regular solution of the Coulomb wave equation can be expressed by the imaginary part of the irregular solution, or the linear combination of the two independent irregular solutions, and indeed one can find similarities between this expression and the reported

expressions for the Gordon's integral. Then we showed that this formula excellently reproduces the phase and the Fano's propensity rule in the continuum-continuum transition, compared to the TDSE and other theoretical approaches. In addition, we modified the WKB asymptotic approximation by expanding the terms to  $r^{-1}$ , to which the centrifugal potential contributes. The Fano's propensity rule and the main feature of the phases in continuum-continuum transitions can be nicely captured with this relatively simple expression that involves only the gamma function. Finally, we used our method to calculate the relative RABBIT phases between the co- and counter-rotating XUV and IR at different electron emission angles. Even at kinetic energy as low as 3.3 eV, our proposed analytical formula quantitatively agrees with both the TDSE calculation and the experimental values. We also checked the case with the shifted expansion center for calculating the spherical harmonics, and the results indicates that our method is not very sensitive to the shape of the short-range potential field, which opens the possibility of adapting our method to molecules.

## Acknowledgements

We thank David Busto and Mathieu Gisselbrecht for fruitful discussions. This work was funded by ETH Zürich. J.-B. Ji acknowledges the funding from the ETH grant 41-20-2. M. H.'s work was funded by the European Union's Horizon 2020 research and innovation program under Marie Skłodowska-Curie agreement grant No. 801459, FP-RESOMUS.

## References

- [1] Nobel Prize Outreach AB 2024 2024 The Nobel Prize in Physics 2023. Nobelprize.org <https://www.nobelprize.org/prizes/physics/2023/summary/> [Accessed 05-07-2024]
- [2] McPherson A, Gibson G, Jara H, Johann U, Luk T S, McIntyre I A, Boyer K and Rhodes C K 1987 *JOSA B* **4** 595
- [3] Ferray M, L'Huillier A, Li X F, Lompre L A, Mainfray G and Manus C 1988 *J. Phys. B* **21** L31
- [4] Itatani J, Quéré F, Yudin G L, Ivanov M Y, Krausz F and Corkum P B 2002 *Phys. Rev. Lett.* **88** 173903
- [5] Kienberger R, Goulielmakis E, Uiberacker M, Baltuska A, Yakovlev V, Bammer F, Scrinzi A, Westerwalbesloh T, Kleineberg U, Heinzmann U, Drescher M and Krausz F 2003 *Nature* **427** 817–821
- [6] Gaumnitz T, Jain A, Pertot Y, Huppert M, Jordan I, Ardana-Lamas F and Wörner H J 2017 *Optics Express* **25** 27506–27518
- [7] Paul P M, Toma E S, Breger P, Mullot G, Augé F, Balcou P, Muller H G and Agostini P 2001 *Science* **292** 1689
- [8] Muller H 2002 *Applied Physics B* **74** s17–s21 ISSN 1432-0649 URL <https://doi.org/10.1007/s00340-002-0894-8>
- [9] Dörner R, Mergel V, Jagutzki O, Spielberger L, Ullrich J, Moshhammer R and Schmidt-Böcking H 2000 *Physics Reports* **330** 95–192
- [10] Ullrich J, Moshhammer R, Dorn A, Dörner R, Schmidt L and Schmidt-Böcking H 2003 *Rep. Prog. Phys.* **66** 1463
- [11] Gong X, Heck S, Jelovina D, Perry C, Zinchenko K, Lucchese R and Wörner H J 2022 *Nature* **609** 507–511

- [12] Eisenbud L 1948 *The formal properties of nuclear collisions* (Princeton University)
- [13] Wigner E P 1955 *Phys Rev A* **98** 145
- [14] Smith F T 1960 *Phys. Rev.* **118** 349–356 URL <http://link.aps.org/doi/10.1103/PhysRev.118.349>
- [15] Amusia M Y, Ivanov V, Cherepkov N and Chernysheva L 1972 *Physics Letters A* **40** 361–362
- [16] Kheifets A S 2013 *Phys. Rev. A* **87** 063404– URL <http://link.aps.org/doi/10.1103/PhysRevA.87.063404>
- [17] Zangwill A and Soven P 1980 *Physical Review A* **21** 1561
- [18] Dixit G, Chakraborty H S and Madjet M E A 2013 *Physical review letters* **111** 203003
- [19] Gianturco F A, Lucchese R R and Sanna N 1994 *J. Chem. Phys.* **100** 6464–6471 URL <http://link.aip.org/link/?JCP/100/6464/1>
- [20] Natalense A P P and Lucchese R R 1999 *J. Chem. Phys.* **111** 5344–5348 URL <http://link.aip.org/link/?JCP/111/5344/1>
- [21] Busto D, Zhong S, Dahlström J M, L’Huillier A and Gisselbrecht M 2024 *Ultrafast Electronic and Structural Dynamics* (Singapore: Springer Nature Singapore) chap 1, pp 1–43
- [22] Dahlström J, Guénot D, Klünder K, Gisselbrecht M, Mauritsson J, L’Huillier A, Maquet A and Taïeb R 2013 *Chemical Physics* **414** 53–64 ISSN 0301-0104 URL <http://www.sciencedirect.com/science/article/pii/S0301010412000298>
- [23] Dahlström J M, L’Huillier A and Maquet A 2012 *Journal of Physics B: Atomic, Molecular and Optical Physics* **45** 183001 ISSN 0953-4075 URL <http://stacks.iop.org/0953-4075/45/i=18/a=183001>
- [24] Marante C, Argenti L and Martín F 2014 *Physical Review A* **90** 012506
- [25] Klünder K, Dahlström J M, Gisselbrecht M, Fordell T, Swoboda M, Guénot D, Johnsson P, Caillat J, Mauritsson J, Maquet A, Taïeb and L’Huillier A 2011 *Physical Review Letters* **106**(14) 143002 URL <http://link.aps.org/doi/10.1103/PhysRevLett.106.143002>
- [26] Guénot D, Klünder K, Arnold C L, Kroon D, Dahlström J M, Miranda M, Fordell T, Gisselbrecht M, Johnsson P, Mauritsson J, Lindroth E, Maquet A, Taïeb R, L’Huillier A and Kheifets A S 2012 *Phys. Rev. A* **85**(5) 053424 URL <http://link.aps.org/doi/10.1103/PhysRevA.85.053424>
- [27] Huppert M, Jordan I, Baykusheva D, Von Conta A and Wörner H J 2016 *Physical Review Letters* **117** 093001
- [28] Baykusheva D and Wörner H J 2017 *The Journal of Chemical Physics* **146** 124306 ISSN 0021-9606 URL <http://dx.doi.org/10.1063/1.4977933>
- [29] Isinger M, Squibb R, Busto D, Zhong S, Harth A, Kroon D, Nandi S, Arnold C, Miranda M, Dahlström J M *et al.* 2017 *Science* **358** 893–896
- [30] Heck S, Baykusheva D, Han M, Ji J B, Perry C, Gong X and Wörner H J 2021 *Science Advances* **7** eabj8121
- [31] Jordan I, Huppert M, Rattenbacher D, Peper M, Jelovina D, Perry C, von Conta A, Schild A and Wörner H J 2020 *Science* **369** 974–979 ISSN 0036-8075 (*Preprint* <https://science.sciencemag.org/content/369/6506/974.full.pdf>) URL <https://science.sciencemag.org/content/369/6506/974>
- [32] Heck S, Han M, Jelovina D, Ji J B, Perry C, Gong X, Lucchese R, Ueda K and Wörner H J 2022 *Physical Review Letters* **129** 133002
- [33] Fuchs J, Douguet N, Donsa S, Martin F, Burgdörfer J, Argenti L, Cattaneo L and Keller U 2020 *Optica* **7** 154–161
- [34] Busto D, Vinbladh J, Zhong S, Isinger M, Nandi S, Maclot S, Johnsson P, Gisselbrecht M, L’Huillier A, Lindroth E *et al.* 2019 *Physical review letters* **123** 133201
- [35] Han M, Ji J B, Leung C S, Ueda K and Wörner H J 2024 *Science Advances* **10** eadj2629
- [36] Boll D I R, Martini L and Fojon O A 2022 *Physical Review A* **106** 023116
- [37] Boll D I R, Martini L, Palacios A and Fojon O A 2023 *Physical Review A* **107** 043113
- [38] Aymar M and Crance M 1980 *Journal of Physics B: Atomic and Molecular Physics* **13** L287
- [39] Shakeshaft R 1986 *Physical Review A* **34** 244



- [40] NIST Digital Library of Mathematical Functions <https://dlmf.nist.gov/>, Release 1.2.1 of 2024-06-15 f. W. J. Olver, A. B. Olde Daalhuis, D. W. Lozier, B. I. Schneider, R. F. Boisvert, C. W. Clark, B. R. Miller, B. V. Saunders, H. S. Cohl, and M. A. McClain, eds. URL <https://dlmf.nist.gov/>
- [41] Gaspard D 2018 *Journal of Mathematical Physics* **59**
- [42] Shakeshaft R 1985 *Journal of Physics B: Atomic and Molecular Physics* **18** L611
- [43] Meixner J 1933 *Mathematische Zeitschrift* **36** 677–707
- [44] Hostler L 1964 *Journal of Mathematical Physics* **5** 591–611
- [45] Hostler L C 1970 *Journal of Mathematical Physics* **11** 2966–2970
- [46] Zorich V A 2016 *Integrals Depending on a Parameter* (Berlin, Heidelberg: Springer Berlin Heidelberg) pp 405–492 ISBN 978-3-662-48993-2 URL [https://doi.org/10.1007/978-3-662-48993-2\\_9](https://doi.org/10.1007/978-3-662-48993-2_9)
- [47] Gordon W 1929 *Annalen der Physik* **394** 1031–1056
- [48] Tarasov V 1995 *International Journal of Modern Physics B* **9** 2699–2718
- [49] Tarasov V 2003 *Journal of Mathematical Physics* **44** 1449–1452
- [50] Saad N and Hall R L 2003 *Journal of Physics A: Mathematical and General* **36** 7771
- [51] Wolfram Research I 2024 The mathematical functions site <https://functions.wolfram.com/> (Accessed on 07/01/2024)
- [52] Bateman H and Erdélyi A 1955 *Higher transcendental functions (California Institute of technology. Bateman Manuscript project no 1)* (New York, NY: McGraw-Hill) URL <https://cds.cern.ch/record/100233>
- [53] Karule E 1978 *Journal of Physics B: Atomic and Molecular Physics* **11** 441
- [54] Karule E and Moine B 2003 *Journal of Physics B: Atomic, Molecular and Optical Physics* **36** 1963
- [55] Dubuc S 1990 *Journal of mathematical analysis and applications* **146** 461–468
- [56] Dahlström J M, Carette T and Lindroth E 2012 *Physical Review A - Atomic, Molecular, and Optical Physics* **86** 1–4 ISSN 10502947
- [57] Oliphant T E 2007 *Computing in science & engineering* **9** 10–20
- [58] Harris C R, Millman K J, Van Der Walt S J, Gommers R, Virtanen P, Cournapeau D, Wieser E, Taylor J, Berg S, Smith N J *et al.* 2020 *Nature* **585** 357–362
- [59] The mpmath development team 2023 *mpmath: a Python library for arbitrary-precision floating-point arithmetic (version 1.3.0)* <http://mpmath.org/>
- [60] Jayadevan A and Thayyullathil R B 2001 *Journal of Physics B: Atomic, Molecular and Optical Physics* **34** 699
- [61] Bray A W, Naseem F and Kheifets A S 2018 *Physical Review A* **97** 1–12 ISSN 24699934
- [62] Jiang W, Armstrong G S, Tong J, Xu Y, Zuo Z, Qiang J, Lu P, Clarke D D, Benda J, Fleischer A *et al.* 2022 *Nature Communications* **13** 5072
- [63] Han M, Ji J B, Balčiūnas T, Ueda K and Wörner H J 2023 *Nature Physics* **19** 230–236
- [64] Han M, Ji J B, Ueda K and Wörner H J 2023 *Optica* **10** 1044–1052
- [65] Villeneuve D, Hockett P, Vrakking M and Niikura H 2017 *Science* **356** 1150–1153